

Weak lensing by triaxial galaxy clusters

F. Feroz^{*} and M. P. Hobson

Astrophysics Group, Cavendish Laboratory, JJ Thomson Avenue, Cambridge CB3 0HE, UK

Accepted —. Received —; in original form 11 August 2011

ABSTRACT

Weak gravitational lensing studies of galaxy clusters often assume a spherical cluster model to simplify the analysis, but some recent studies have suggested this simplifying assumption may result in large biases in estimated cluster masses and concentration values, since clusters are expected to exhibit triaxiality. Several such analyses have, however, quoted expressions for the spatial derivatives of the lensing potential in triaxial models, which are open to misinterpretation. In this paper, we give a clear description of weak lensing by triaxial NFW galaxy clusters and also present an efficient and robust method to model these clusters and obtain parameter estimates. By considering four highly triaxial NFW galaxy clusters, we re-examine the impact of the simplifying assumption of sphericity and find that while the concentration estimates are largely unbiased, except in one of our triaxial NFW simulated clusters, the masses are significantly biased, by up to 40%, for all the clusters we analysed. Moreover, we find that erroneously assuming spherical symmetry can lead to the mistaken conclusion that some substructure is present in the galaxy clusters or, even worse, that multiple galaxy clusters are present in the field. Our cluster fitting method also allows one to answer the question of whether a given cluster exhibits triaxiality or a simple spherical model is good enough.

Key words: methods: data analysis – methods: statistical – cosmology: observations – galaxies: clusters: general

1 INTRODUCTION

Clusters of galaxies are the most massive gravitationally bound objects in the universe and, as such, are critical tracers of the formation of large-scale structure. The number counts of clusters as a function of their mass and redshift have been predicted both analytically (see e.g. Press & Schechter 1974; Sheth et al. 2001) and from large scale numerical simulations (see e.g. Jenkins et al. 2001; Evrard et al. 2002), and are particularly sensitive to the cosmological parameters σ_8 and Ω_m (see e.g. Battye & Weller 2003). The size and formation history of massive clusters is such that the ratio of gas mass to total mass is expected to be representative of the universal ratio Ω_b/Ω_m , once the relatively small amount of baryonic matter in the cluster galaxies is taken into account (see e.g. White et al. 1993).

The study of cosmic shear has progressed rapidly in recent years, with the availability of high quality wide-field lensing data. Large dedicated surveys with ground-based telescopes have been employed to reconstruct the mass distribution of the universe and constrain cosmological parameters (see e.g. Massey et al. 2007, 2005; Hoekstra et al. 2006). Weak lensing also allows one to detect galaxy clusters without making any assumptions about the baryon fraction, richness, morphology or dynamical state of the cluster, and so weak lensing cluster modelling would allow one to

test these assumptions by observing the cluster with optical, X-ray or Sunyaev–Zel’dovich (SZ) methods. Nonetheless, weak lensing studies are very challenging, not only because the data are very noisy, but also because of the inherent under-determined nature of the problem, namely constraining the 3-D structure of the galaxy cluster using lensing observations that are sensitive only to the 2-D projected mass distribution, at least in the thin lens approximation.

A model cluster density profile can be determined from numerical N -body simulations of large-scale structure formation in a Λ CDM universe. In particular, assuming spherical symmetry, the NFW profile (Navarro et al. 1997) provides a good fit to the simulations. The NFW profile is parameterized by the virial mass M_{200} and the concentration parameter C , which are highly-correlated. The concentration parameter is directly related to the central density of the cluster, which depends on cluster’s formation history. Since galaxy clusters are the most recently bound objects in the universe, the cluster concentrations serve as probes of the mean density of the universe at lower redshifts. N -body simulations predict $C \sim 4$ for a cluster of mass $M_{200} = 10^{15} h^{-1} M_\odot$. Several studies, assuming a spherical NFW model, have reported weak lensing results with very high concentration values of $C \sim 8$ (see e.g. Limousin et al. 2007; Kneib et al. 2003; Gavazzi et al. 2003), casting doubt on the Λ CDM model. In order to shed further light on this discrepancy, it is important to understand to what extent can these results be explained by deviations from spherical symmetry. Another reason for studying the triaxiality of galaxy clusters is

^{*} E-mail: f.feroz@mrao.cam.ac.uk

that several studies on structure formation in Λ CDM suggest clusters often exhibit significant triaxiality (see e.g. Bett et al. (2007); Shaw et al. (2006)).

Several attempts have already been made towards understanding the impact of triaxiality in explaining the deviations from Λ CDM of the observed gravitational lensing results. Jing & Suto (2002) first presented a full parameterization for a triaxial NFW halo. Oguri et al. (2005) and Gavazzi (2005) showed that a triaxial NFW fit to gravitational lensing observations of clusters Abell 1689 and MS2137-23 yields parameter estimates consistent with N -body simulation. Corless & King (2007) and Corless & King (2008) presented a general Markov Chain Monte Carlo (MCMC) method for fitting a triaxial NFW model to weak lensing observations. From the analysis of simulated lensing observations of triaxial clusters, they concluded that significant elongation of the cluster along the line of sight can cause its mass to be overestimated by up to 50 per cent and its concentration by as much as a factor of 2, if one simply assumes a spherical NFW model when analysing its lensing signal. This claim is important since it would significantly ease the tension between the Λ CDM model and the very high values of the concentration parameter reported in a number of clusters, derived from lensing observations assuming a spherical NFW model.

The triaxial lensing equations quoted in Corless & King (2007) and Corless & King (2008) adopted the triaxial NFW model equations from Keeton (2001), which can easily be misinterpreted, and also had some additional errors, although the correct form of equations were used in their analysis code (King, private communication). In any case, our purpose in this paper is to present a clear description of the weak lensing equations for the triaxial NFW model and simultaneously introduce an efficient, robust and accurate method, based on nested sampling, for fitting triaxial NFW model to weak lensing observations. In particular, we study the discrepancies that may arise in fitting a spherical NFW model to a galaxy cluster exhibiting significant triaxiality.

The outline of this letter is as follows. In Sec. 2 we introduce Bayesian inference, which we use for cluster fitting. In Sec. 3 we describe the triaxial NFW model and derive the relevant equations. We apply our method to a set of simulated weak lensing simulations in Sec. 4. Finally we present our conclusions in Sec. 5.

2 BAYESIAN INFERENCE

Our cluster fitting methodology is built upon the principles of Bayesian inference, which provides a consistent approach to the estimation of a set of parameters Θ in a model (or hypothesis) H for the data \mathbf{D} . Bayes' theorem states that

$$\Pr(\Theta|\mathbf{D}, H) = \frac{\Pr(\mathbf{D}|\Theta, H) \Pr(\Theta|H)}{\Pr(\mathbf{D}|H)}, \quad (1)$$

where $\Pr(\Theta|\mathbf{D}, H) \equiv P(\Theta)$ is the posterior probability distribution of the parameters, $\Pr(\mathbf{D}|\Theta, H) \equiv \mathcal{L}(\Theta)$ is the likelihood, $\Pr(\Theta|H) \equiv \pi(\Theta)$ is the prior, and $\Pr(\mathbf{D}|H) \equiv \mathcal{Z}$ is the Bayesian evidence.

In parameter estimation, the normalising evidence factor is usually ignored, since it is independent of the parameters Θ , and inferences are obtained by taking samples from the (unnormalised) posterior using standard MCMC sampling methods, where at equilibrium the chain contains a set of samples from the parameter space distributed according to the posterior. This posterior constitutes the complete Bayesian inference of the parameter values, and

can be marginalised over each parameter to obtain individual parameter constraints.

In contrast to parameter estimation problems, for model selection the evidence takes the central role and is simply the factor required to normalize the posterior over Θ :

$$\mathcal{Z} = \int \mathcal{L}(\Theta) \pi(\Theta) d^D \Theta, \quad (2)$$

where D is the dimensionality of the parameter space. As the average of the likelihood over the prior, the evidence is larger for a model if more of its parameter space is likely and smaller for a model with large areas in its parameter space having low likelihood values, even if the likelihood function is very highly peaked. Thus, the evidence automatically implements Occam's razor. The question of model selection between two models H_0 and H_1 can then be decided by comparing their respective posterior probabilities given the observed data set \mathbf{D} , as follows

$$R = \frac{\Pr(H_1|\mathbf{D})}{\Pr(H_0|\mathbf{D})} = \frac{\Pr(\mathbf{D}|H_1) \Pr(H_1)}{\Pr(\mathbf{D}|H_0) \Pr(H_0)} = \frac{\mathcal{Z}_1 \Pr(H_1)}{\mathcal{Z}_0 \Pr(H_0)}, \quad (3)$$

where $\Pr(H_1)/\Pr(H_0)$ is the a priori probability ratio for the two models, which can often be set to unity but occasionally requires further consideration.

Evaluation of the multidimensional integral in (2) is a challenging numerical task. Standard techniques like thermodynamic integration are extremely computationally intensive which makes evidence evaluation at least an order of magnitude more costly than parameter estimation. Some fast approximate methods have been used for evidence evaluation, such as treating the posterior as a multivariate Gaussian centred at its peak (see e.g. Hobson & McLachlan 2003), but this approximation is clearly a poor one for multimodal posteriors (except perhaps if one performs a separate Gaussian approximation at each mode). The Savage-Dickey density ratio has also been proposed (see e.g. Trotta 2007) as an exact, and potentially faster, means of evaluating evidences, but is restricted to the special case of nested hypotheses and a separable prior on the model parameters. Various alternative information criteria for astrophysical model selection are discussed by Liddle (2007), but the evidence remains the preferred method.

The nested sampling approach, introduced by Skilling (2004), is a Monte Carlo method targeted at the efficient calculation of the evidence, but also produces posterior inferences as a by-product. Feroz & Hobson (2008) and Feroz et al. (2009) built on this nested sampling framework and have introduced the MULTINEST algorithm which is very efficient in sampling from posteriors that may contain multiple modes and/or large (curving) degeneracies and also calculates the evidence. This technique has greatly reduced the computational cost of Bayesian parameter estimation and model selection, and is employed in this paper.

3 WEAK LENSING BY TRIAXIAL GALAXY CLUSTERS

3.1 Weak lensing background

A cluster mass distribution is investigated using weak gravitational lensing through the relationship (see e.g. Schramm & Kayser 1995) $\langle \epsilon(\mathbf{x}) \rangle = g(\mathbf{x})$, that is, at any point \mathbf{x} on the sky, the local average of the complex ellipticities $\epsilon = \epsilon_1 + i\epsilon_2$ of a collection of background galaxy images is an unbiased estimator of the local complex reduced shear field, $g = g_1 + ig_2$, due to the cluster. Adopting the thin-lens approximation, for a projected mass distribution $\Sigma(\mathbf{x})$ in

the lens, the reduced shear $g(\mathbf{x})$ is defined as

$$g(\mathbf{x}) = \frac{\gamma(\mathbf{x})}{1 - \kappa(\mathbf{x})}, \quad (4)$$

where the convergence $\kappa(\mathbf{x}) = \Sigma(\mathbf{x})/\Sigma_{\text{crit}}$ and the shear $\gamma(\mathbf{x})$ can, in general, be written as a convolution integral over the convergence $\kappa(\mathbf{x})$ (see e.g. Bridle et al. 1998). Σ_{crit} is the critical surface mass density

$$\Sigma_{\text{crit}} = \frac{c^2}{4\pi G} \frac{D_s}{D_l D_{ls}}, \quad (5)$$

where D_s , D_l and D_{ls} are the angular-diameter distances between, respectively, the observer and each galaxy, the observer and the lens, and the lens and each galaxy. In general, the redshifts of each background galaxy can be different, but are assumed to be known. The lensing effect is weak or strong if $\kappa \ll 1$ or $\kappa \gtrsim 1$ respectively. The observed ellipticity $\epsilon(\mathbf{x})$ can be converted to source ellipticity (i.e. prior to lensing) $\epsilon^s(\mathbf{x})$ as follows (Seitz & Schneider 1997):

$$\epsilon^s(\mathbf{x}) = \begin{cases} \frac{\epsilon(\mathbf{x}) - g(\mathbf{x})}{1 - g^*(\mathbf{x})\epsilon(\mathbf{x})} & (|g| \leq 1) \\ \frac{1 - g(\mathbf{x})\epsilon^*(\mathbf{x})}{\epsilon^*(\mathbf{x}) - g^*(\mathbf{x})} & (|g| > 1) \end{cases}, \quad (6)$$

where an asterisk denotes complex conjugation. The inverse transformation can be obtained by swapping $\epsilon^s(\mathbf{x})$ with $\epsilon(\mathbf{x})$ and by replacing $g(\mathbf{x})$ with $-g(\mathbf{x})$.

The number count of the background galaxies is changed by lensing due to two competing effects: (a) some faint sources in highly magnified regions are made brighter and pushed over the flux limit, but (b) the same sources are stretched across the sky reducing the number count of these sources. The observed number density of sources, n is related to the actual background number density n_0 by the flux limit α through $n = n_0 \mu^{\alpha-1}$, where μ is the lensing magnification defined by $\mu^{-1} = (1 - \kappa)^2 - |\gamma|^2$.

3.2 Triaxial NFW model

A model cluster density profile can be determined from numerical N -body simulations of large-scale structure formation in a Λ CDM universe. In particular the NFW profile (Navarro et al. 1997) provides a good fit to the simulations. Assuming spherical symmetry, the NFW profile is given by:

$$\rho(r) = \frac{\rho_s}{(r/r_s)(1 + r/r_s)^2}, \quad (7)$$

where r_s and ρ_s are the radius and density at which the logarithmic slope breaks from -1 to -3 . The extension to a triaxial cluster is performed simply by defining the triaxial radius r , such that

$$r^2 = \frac{X^2}{a^2} + \frac{Y^2}{b^2} + \frac{Z^2}{c^2}, \quad (a \leq b \leq c = 1), \quad (8)$$

where the coordinates X , Y and Z lie along the principal axes of the cluster, and a , b and c are the semi-minor, semi-intermediate and semi-major axes respectively of the iso-density ellipsoid $r = 1$. We define M_{200} as the mass contained within the triaxial radius $r = r_{200}$ at which the density is 200 times the cosmological critical density ρ_{crit} at the redshift of the cluster. The concentration parameter C is a measure of the halo concentration and is defined as $C = r_{200}/r_s$.

Following Oguri et al. (2003), we define the orientation angles (θ, ϕ) such that they represent the polar angles of the line-of-sight of the observer, as measured in the principal coordinate system of the triaxial cluster. We set the semi-major axis $c = 1$ and therefore

the parameters a and b serve as the minor:major and intermediate:major axis ratios respectively. Thus, for a triaxial NFW, cluster parameters are $\Theta = (x_0, y_0, a, b, \theta, \phi, M_{200}, C, z)$, where x_0 and y_0 are the spatial coordinates in the observers xy -plane at which the cluster is centred, and z is its redshift.

The projected surface mass density of a triaxial cluster will have elliptical symmetry and by translating the observer's xy -plane such that the cluster centre is at the origin, and subsequently rotating the coordinate system by the position angle ψ of the iso-surface-density ellipses, the elliptical radius ζ , in the resulting (\bar{x}, \bar{y}) coordinate system, can be written as

$$\zeta^2 = \frac{\bar{x}^2}{q_x^2} + \frac{\bar{y}^2}{q_y^2}, \quad (9)$$

where q_x and q_y are the semi-major and semi-minor axes, respectively, of the ellipse $\zeta = 1$, which corresponds to the projection of the ellipsoid $r = 1$. The position angle ψ is given by

$$\psi = \frac{1}{2} \arctan \left(\frac{B}{A - C} \right), \quad (10)$$

and the projected axis ratios read

$$q_x^2 = \frac{2f}{A + C - \sqrt{(A - C)^2 + B^2}}, \quad (11)$$

$$q_y^2 = \frac{2f}{A + C + \sqrt{(A - C)^2 + B^2}}, \quad (12)$$

where

$$f = \sin^2 \theta \left(\frac{c^2}{a^2} \cos^2 \phi + \frac{c^2}{b^2} \sin^2 \phi \right) + \cos^2 \theta, \quad (13)$$

$$A = \cos^2 \theta \left(\frac{c^2}{a^2} \sin^2 \phi + \frac{c^2}{b^2} \cos^2 \phi \right) + \frac{c^2}{a^2} \frac{c^2}{b^2} \sin^2 \theta, \quad (14)$$

$$B = \cos \theta \sin 2\phi \left(\frac{c^2}{a^2} - \frac{c^2}{b^2} \right), \quad (15)$$

$$C = \frac{c^2}{b^2} \sin^2 \phi + \frac{c^2}{a^2} \cos^2 \phi. \quad (16)$$

Note that $q_x \geq q_y$ for the given rotation angle ψ . We define the axis ratio q as $q = q_y/q_x$, which defines the ellipticities of the projected iso-density contours of the triaxial cluster.

The lensing shear fields $\bar{\gamma}_1(\bar{x}, \bar{y})$ and $\bar{\gamma}_2(\bar{x}, \bar{y})$, and convergence $\bar{\kappa}(\bar{x}, \bar{y})$ in the (\bar{x}, \bar{y}) coordinate system can be calculated as the second derivatives of the lensing potential $\bar{\Phi}(\bar{x}, \bar{y}) = \Phi(x, y)$ as follows (with commas indicating differentiation):

$$\bar{\gamma}_1 = \frac{1}{2} (\bar{\Phi}_{,\bar{x}\bar{x}} - \bar{\Phi}_{,\bar{y}\bar{y}}), \quad (17)$$

$$\bar{\gamma}_2 = \bar{\Phi}_{,\bar{x}\bar{y}}, \quad (18)$$

$$\bar{\kappa} = \frac{1}{2} (\bar{\Phi}_{,\bar{x}\bar{x}} + \bar{\Phi}_{,\bar{y}\bar{y}}). \quad (19)$$

In order to apply the method of Schramm (1990) and Keeton (2001) to evaluate these lensing formulae, it is necessary, however, to perform a further coordinate scaling $\bar{\bar{x}} = \bar{x}/q_x$, $\bar{\bar{y}} = \bar{y}/q_x$ such that the elliptical radius can be written as

$$\zeta^2 = \bar{\bar{x}}^2 + \frac{\bar{\bar{y}}^2}{q^2}, \quad (20)$$

and so the semi-major axis of the ellipse $\zeta = 1$ is equal to unity.

In the $(\bar{\bar{x}}, \bar{\bar{y}})$ coordinate system, one can now express the sec-

ond derivatives of the lensing potential $\bar{\Phi}(\bar{x}, \bar{y})$ as follows¹:

$$\bar{\Phi}_{,\bar{x}\bar{x}}(\bar{x}, \bar{y}) = q\bar{x}^2 K_0(\bar{x}, \bar{y}) + qJ_0(\bar{x}, \bar{y}), \quad (21)$$

$$\bar{\Phi}_{,\bar{y}\bar{y}}(\bar{x}, \bar{y}) = q\bar{y}^2 K_2(\bar{x}, \bar{y}) + qJ_1(\bar{x}, \bar{y}), \quad (22)$$

$$\bar{\Phi}_{,\bar{x}\bar{y}}(\bar{x}, \bar{y}) = q\bar{x}\bar{y}K_1(\bar{x}, \bar{y}), \quad (23)$$

where

$$K_n(\bar{x}, \bar{y}) = \int_0^1 \frac{u\kappa'(\zeta(u))}{\zeta(u)[1 - (1 - q^2)u]^{n+1/2}} du, \quad (24)$$

$$J_n(\bar{x}, \bar{y}) = \int_0^1 \frac{\kappa(\zeta(u))}{[1 - (1 - q^2)u]^{n+1/2}} du, \quad (25)$$

in which

$$\zeta(u)^2 = u \left(\bar{x}^2 + \frac{\bar{y}^2}{1 - (1 - q^2)u} \right), \quad (26)$$

and

$$\kappa'(\zeta(u)) = \frac{d\kappa(\zeta(u))}{d\zeta(u)}. \quad (27)$$

The surface mass density $\kappa(\zeta)$ in the above equations can be expressed in terms of the spherical surface mass density $\kappa_s(\zeta)$ (see Bartelmann 1996 for the expression for $\kappa_s(\zeta)$ for the NFW profile) as follows (see Oguri et al. 2003 for the derivation):

$$\kappa(\zeta) = \frac{\kappa_s(\zeta)}{\sqrt{f}}, \quad (28)$$

where f is given in Eq. (13).

The shear and convergence fields in the (\bar{x}, \bar{y}) coordinates, given in Eqs. (17)–(19) are straightforwardly calculated from the derivatives of the lensing potentials Eqs. (21)–(23) using the fact that $\bar{\Phi}_{,\bar{x}\bar{x}}(\bar{x}, \bar{y}) = \bar{\Phi}_{,\bar{x}\bar{x}}(\bar{x}, \bar{y})$, and similarly for the other terms (since the gravitational potential has a scaling dimension of 2). Finally, the convergence and shear values in the observer's original (x, y) coordinate system (shifted such that the cluster centre is at the origin) are obtained by rotating the shear vector by angle ψ , given in Eq. (10), as follows²

$$\kappa(x, y) = \bar{\kappa}(\bar{x}, \bar{y}), \quad (29)$$

$$\gamma_1(x, y) = |\bar{\gamma}(\bar{x}, \bar{y})| \cos(2(\alpha + \psi)), \quad (30)$$

$$\gamma_2(x, y) = |\bar{\gamma}(\bar{x}, \bar{y})| \sin(2(\alpha + \psi)), \quad (31)$$

where

$$|\bar{\gamma}(\bar{x}, \bar{y})| = \sqrt{\bar{\gamma}_1^2(\bar{x}, \bar{y}) + \bar{\gamma}_2^2(\bar{x}, \bar{y})}, \quad (32)$$

and

$$\alpha = \frac{1}{2} \arctan \left(\frac{\bar{\gamma}_2(\bar{x}, \bar{y})}{\bar{\gamma}_1(\bar{x}, \bar{y})} \right). \quad (33)$$

We have tested the triaxial NFW lensing equations given

¹ The expression for the integral $J_n(X, Y)$ in Sec. 4 of Keeton (2001) should have $\kappa(\zeta(u))$ instead of $\kappa(\zeta(u)^2)$, in the numerator.

² Although the description of triaxial lensing in Corless & King (2007) and Corless & King (2008) makes no mention of the successive coordinate rescaling and rotation discussed above, Corless (2008) does mention that all triaxial projections are rotated by their position angle ψ before lensing integrals are calculated and that the resulting shear and convergence values are rotated back to the original orientation of the lens. Also, Eq. (A18) in Corless & King (2008) should not have q_X in the denominator. However, the correct form of equations were used in their analysis code (King, private communication).

above by numerically integrating the mass density of a given triaxial cluster, along the line-of-sight to calculate the surface mass density $\kappa(x, y)$ which was found to be equal to the $\kappa(x, y)$ calculated by using Eqs. (19) and (28).

3.3 Weak lensing likelihood

The observed complex ellipticity components of the N_{gal} background galaxies can be ordered into a data vector \mathbf{d} with components

$$d_i = \begin{cases} \text{Re}(\epsilon_i) & (i \leq N_{\text{gal}}) \\ \text{Im}(\epsilon_{i-N_{\text{gal}}}) & (N_{\text{gal}} + 1 \leq i \leq 2N_{\text{gal}}) \end{cases}. \quad (34)$$

Likewise the corresponding components of the complex reduced shear $g(\mathbf{x}_i)$ at each galaxy position, as predicted by the cluster model, can be arranged into the predicted data vector \mathbf{d}^P , with the arrangement of components matching (34).

The uncertainty on the components (i.e. real and imaginary parts) of the measured ellipticity ϵ consists of two contributions. The components of the intrinsic ellipticity, ϵ_s , of the background galaxies (i.e. prior to lensing) may be taken as having been drawn independently from a Gaussian distribution with mean zero and variance σ_{int}^2 . If we denote distribution of ϵ_s by $p_{\text{int}}(\epsilon_s)$, the distribution of the lensed ellipticities $p_{\epsilon_\ell}(\epsilon_\ell)$ is then given by:

$$p_{\epsilon_\ell}(\epsilon_\ell) = p_{\text{int}}(\epsilon_s) \left| \frac{d\epsilon_s}{d\epsilon_\ell} \right|^2, \quad (35)$$

where we have taken account of ϵ_s and ϵ_ℓ both being complex variables. The Jacobian determinant can be found using Eq.(6) and is given by:

$$\left| \frac{d\epsilon_s}{d\epsilon_\ell} \right| = \begin{cases} \frac{1-|g|^2}{|\epsilon_\ell g^* - 1|^2} & (|g| \leq 1) \\ \frac{|g|^2 - 1}{|\epsilon_\ell - g|^2} & (|g| > 1) \end{cases}. \quad (36)$$

The second source of uncertainty on the measured ellipticity is due to the errors introduced by the galaxy shape estimation procedure, such that $\epsilon = \epsilon_\ell + \Delta\epsilon_\ell$, where the components of $\Delta\epsilon_\ell$ can be modelled as drawn from a Gaussian with mean zero and variance σ_{obs}^2 . Denoting this distribution by $p_{\text{obs}}(\Delta\epsilon_\ell)$, the probability distribution for the measured ellipticities can be obtained as follows:

$$p_\epsilon(\epsilon) = \int p_{\epsilon_\ell}(\epsilon_\ell) p_{\text{obs}}(\epsilon - \epsilon_\ell) d\epsilon_\ell. \quad (37)$$

If the reduced shear is small i.e. for $|g| \ll 1$, the Jacobian determinant in Eq. (36) reduces to unity and we have $p_{\epsilon_\ell}(\epsilon_\ell) = p_{\text{int}}(\epsilon_s)$. This reduces Eq. (37) to a convolution of two Gaussians with means zero and standard deviations σ_{int} and σ_{obs} respectively. Consequently $p_\epsilon(\epsilon)$ is a Gaussian with mean zero and standard deviation σ_i corresponding to the i th galaxy, given by:

$$\sigma_i^2 = \sigma_{\text{obs}}^2 + \sigma_{\text{int}}^2. \quad (38)$$

This leads to a diagonal noise covariance matrix \mathbf{C} on the ellipticity components. This is however, not the case when $|g| \simeq 1$. Since the expected reduced shear from the low redshift simulated clusters in this study is not too large, we adopt this approximation.

As shown by Marshall et al. (2003), we can then write the likelihood function as $\mathcal{L}(\Theta) = Z_L^{-1} \exp(-\frac{1}{2}\chi^2)$, where χ^2 is the usual misfit statistic

$$\chi^2 = (\mathbf{d} - \mathbf{d}^P)^T \mathbf{C}^{-1} (\mathbf{d} - \mathbf{d}^P) = \sum_{i=1}^{N_{\text{gal}}} \sum_{j=1}^2 \frac{(\epsilon_{j,i} - g_j(\mathbf{x}_i))^2}{\sigma_i^2}, \quad (39)$$

| Parameters | Flat Priors | Bett Priors | Spherical Priors |
|-------------------------|--|--|--|
| x_0 | $-12' \leq x_0 \leq 12'$ | $-12' \leq x_0 \leq 12'$ | $-12' \leq x_0 \leq 12'$ |
| y_0 | $-12' \leq y_0 \leq 12'$ | $-12' \leq y_0 \leq 12'$ | $-12' \leq y_0 \leq 12'$ |
| a/b | $0.2 \leq a/b \leq 1.0$ | 0.800 ± 0.125 | $a/b = 1$ |
| b | $0.2 \leq b \leq 1.0$ | 0.85 ± 0.10 | $b = 1$ |
| θ/rad | $0 \leq \sin(\theta) \leq 1$ | $0 \leq \sin(\theta) \leq 1$ | $\theta = 0$ |
| ϕ/rad | $0 \leq \phi \leq 2\pi$ | $0 \leq \phi \leq 2\pi$ | $\phi = 0$ |
| $M_{200}/h^{-1}M_\odot$ | $14.0 \leq \log_{10}(M_{200}) \leq 16$ | $14.0 \leq \log_{10}(M_{200}) \leq 16$ | $14.0 \leq \log_{10}(M_{200}) \leq 16$ |
| C | $0 \leq C \leq 15$ | $0 \leq C \leq 15$ | $0 \leq C \leq 15$ |
| z | $z = 0.2$ | $z = 0.2$ | $z = 0.2$ |

Table 1. Priors for the cluster parameters. Inequalities denote uniform prior probability between the given limits, equalities mean delta function priors, and $(a \pm b)$ denotes a Gaussian prior with mean a and variance b^2 .

and the normalisation factor is $Z_L = (2\pi)^{2N_{\text{gal}}/2} |\mathbf{C}|^{1/2}$. Note that it is necessary to include this normalisation factor in the likelihood, since the covariance matrix \mathbf{C} is not constant, but depends on the cluster model parameters through the predicted shear terms in (38).

3.4 Priors on cluster parameters

To determine the model completely it only remains to specify the prior $\pi(\Theta)$ on the cluster parameters $\Theta = (x_0, y_0, a, b, \theta, \phi, M_{200}, C, z)$. The choice of prior is particularly important for weak lensing analysis since the problem is inherently underconstrained and therefore any prior information available about the cluster parameter is extremely useful. One should however be careful in the choice of priors not to impose too strong assumptions which may lead to erroneous inferences.

We use three different priors which we call flat, Bett and spherical. These priors are specified in Tab. 1. In all 3 cases, we assume that cluster redshift is known. It should also be noted that although the orientation angles are defined over $0 < \theta < \pi$ and $0 < \phi < 2\pi$, because of the elliptical nature of the projected density contours, unique lensing profiles are possible only over the range $0 < \theta < \pi/2$ and $0 < \phi < \pi$. Apart from the spherical case, the prior on θ is uniform in $\sin(\theta)$.

The most restrictive case is that of the spherical priors, which assume the axis ratios to be fixed $a = b = 1$, and hence correspond to a spherical cluster model. This is clearly a very strong assumption and there is a debate in the literature whether this assumption is behind the deviations from Λ CDM of the observed gravitational lensing results (see e.g. Corless & King (2007); Oguri et al. (2005); Gavazzi (2005)). The least restrictive case is given by the flat priors, for which assume a uniform prior distribution on the axis ratios with $0.2 \leq b \leq 1.0$ and $0.2 \leq a/b \leq 1.0$. An intermediate choice is to use the distribution of axis ratios derived from N -body simulations as the prior on axis ratios. We therefore also consider the Bett priors specified in Corless & King (2008), for which the distribution of axis ratios is taken from N -body simulations by Bett et al. (2007). Bett priors assume a Gaussian distribution on the axis ratios a/b and b with means and standard deviations given in Tab. 1.

4 APPLICATION TO SIMULATED OBSERVATIONS

4.1 Simulations

Following Corless & King (2008), we simulate prolate ($a = b = 0.4$, i.e. ‘cigar-shaped’) and oblate ($a = 0.4$, $b = 1$, i.e. ‘pancake-shaped’) clusters in two orientations: (a) Line-of-sight (LoS): with

the ‘odd’ axis along the line of sight ($\theta = 0$ for prolate and $\theta = \pi/2$, $\phi = 0$ for oblate), and (b) Plane: with the ‘odd’ axis in the plane of the sky ($\theta = \pi/2$ for prolate and $\theta = \phi = 0$ for oblate). LoS orientation results in spherical projected iso-density contours for our chosen prolate and oblate clusters. In Plane orientation, the projected iso-density contours are elliptical with a position angle ψ of $\pi/2$ and 0, respectively, for prolate and oblate clusters. We also simulate a spherically symmetric cluster ($a = b = 1$) to determine the effects of fitting an (overly complicated) triaxial model to it.

All the simulated clusters were assumed to have the NFW density profile as given in Eq. (7), with $x_0 = 0$, $y_0 = 0$, $M_{200} = 10^{15} h^{-1} M_\odot$, $C = 4$ and $z = 0.2$. The simulations were carried out for a field $12'$ in radius, with background source density $n_0 = 30/\text{arcmin}^2$, typical of ground-based observations. We assume all the background galaxies lie at redshift $z = 1$, this is justified by the low redshift ($z = 0.2$) of the simulated lens. The galaxies are positioned randomly in the field with their shapes drawn from a Gaussian distribution with standard deviation $\sigma_\epsilon = \sqrt{\sigma_{\text{int}}^2 + \sigma_{\text{obs}}^2}$, where σ_{int} and σ_{obs} are the intrinsic and observational dispersion of galaxy shapes as discussed in Sec. 3.3. We set $\sigma_{\text{int}} = 0.2$ and $\sigma_{\text{obs}} = 0.1$. These galaxies are then lensed by the cluster as described in Sec. 3.1. The number density of background galaxies is then reduced according to $n = n_0 \mu^{\alpha-1}$ with the flux limit $\alpha = 0.5$, as in Fort et al. (1997) and Corless & King (2008). Throughout we assume a concordance Λ CDM cosmology ($\Omega_{\text{m},0} = 0.3$, $\Omega_{\Lambda,0} = 0.7$ and $h = 0.7$).

4.2 Analysis and Results

Fig. 1 shows the posterior probability distributions, marginalized in the M_{200} - C plane, obtained using the different priors discussed in Sec. 3.4, for fitting a triaxial NFW model to the triaxial cluster simulations discussed in Sec. 4.1. We also analyse our simulated data-sets assuming the spherical model and include the results in Fig. 1. To emulate the analysis of Corless & King (2007), for the spherical model we further consider the case where one removes the galaxies within $1'$ of the cluster centre to avoid the strong lensing regime and only simulate galaxies out to $7.5'$ from the cluster centre. The results for fitting a triaxial NFW model to a spherical cluster are shown in Fig. 2.

As expected, in all cases the flat priors result in broadest posterior distributions, while the spherical priors give the most constrained posteriors. For the flat priors, we see from Fig. 1 that each posterior distribution contains the true parameter values with the 95 per cent confidence region, except for the prolate LoS cluster which has significantly overestimated values for both M_{200} and

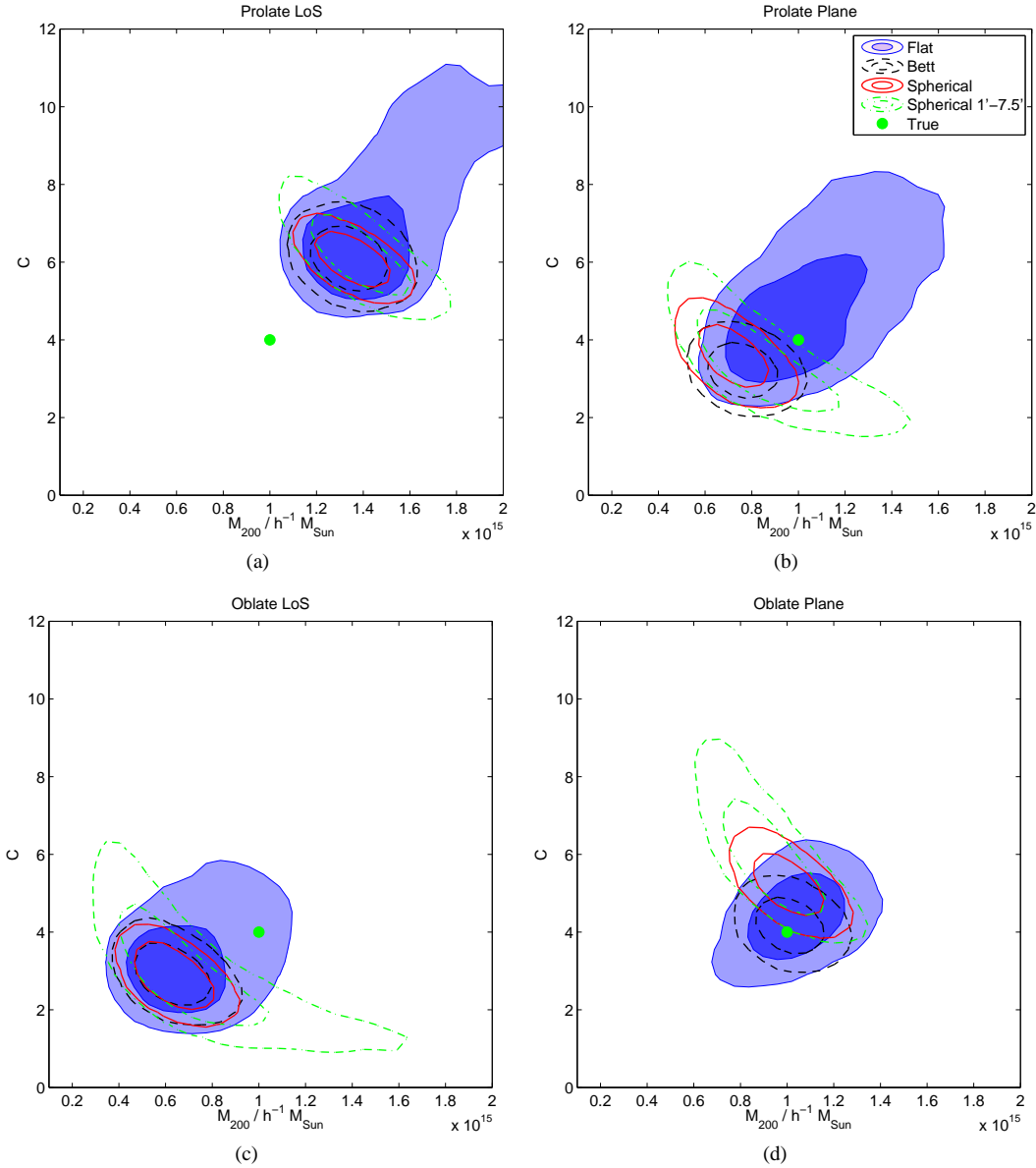


Figure 1. 2-D marginalized posterior probability distributions in the M_{200} - C plane for (a) prolate LoS cluster, (b) prolate plane cluster, (c) oblate LoS cluster and (d) oblate plane cluster. The contours delineate the 68 and 95 per cent confidence regions, respectively, for the different assumed priors.

C . In LoS orientation, the surface mass density of the cluster has spherical symmetry and, coupled with the thin lens approximation, one would expect the axis ratios and orientation angles to be largely unconstrained by the observed galaxy ellipticities. Therefore, the inferences on axis ratios a, b and orientation angles θ, ϕ for our LoS prolate and oblate clusters are expected to be driven by their prior distributions. The overestimation of M_{200} and C for the prolate LoS cluster occurs because it has $\theta = 0$ and $a/b = 1$, which is highly disfavoured by the prior distributions employed. In the absence of strong constraints from the data, the priors thus pull these parameters away from their true values. The consequent inaccuracies in the estimates of θ and a/b result in an overestimation of M_{200} and C . We found that fixing the axis ratios a and b or the orientation angle θ to their true values removes the bias in the estimation of M_{200} and C . The oblate LoS cluster has $\theta = \pi/2, \phi = 0$ which is not disfavoured by the prior distribution and therefore we

do not see a significant bias in the posterior distributions. For the prolate plane and oblate LoS orientations, it is worth noting that the degeneracy directions of the posteriors with flat priors are almost orthogonal to those obtained in these cases by Corless & King (2008) which may be due to the wider priors we used on the axis ratios, whereas the shapes of the posteriors agree well in the other two cases.

As the priors become more restrictive, the true parameter values do begin to fall noticeably outside the two-dimensional 95 per cent confidence region for all cases, except the oblate plane cluster. Even for the spherical priors, however, one obtains largely unbiased estimates for C , except in the prolate LoS orientation for which C is significantly overestimated (as explained above). Turning to M_{200} derived from spherical priors, we see that it is significantly overestimated in the prolate LoS orientation, noticeably underesti-

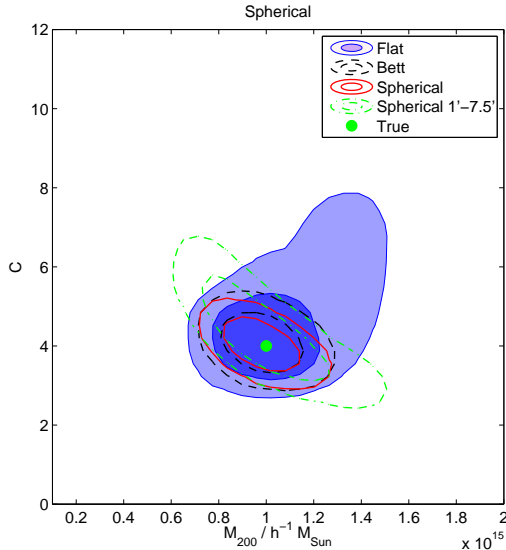


Figure 2. 2-D marginalized posterior probability distributions in the M_{200} - C plane for a spherical cluster.

mated in the oblate LoS case, slightly underestimated in the prolate plane orientation, and largely unbiased for the oblate plane cluster.

The most notable inaccuracies in fitting a spherical NFW model are observed when we allow for more than one spherical cluster in the field. Bayesian model selection can then be used to determine whether multiple spherical clusters provide a better fit to the data. Table 2 lists the Bayesian evidences calculated by our cluster finding algorithm for one triaxial NFW cluster, one spherical NFW cluster and two spherical NFW clusters. As expected, one triaxial NFW cluster model is preferred for the triaxial cluster simulations with their odd axis in the plane of the sky, which results in the surface mass density having elliptical contours. LoS orientation, however, results in spherical projected iso-density contours, as discussed in Sec. 4.1, and since the prior on θ completely rules out the true value for the prolate LoS cluster, there is weak preference for the spherical model over a triaxial cluster model. There is no such mismatch between the true parameter values and the corresponding prior distributions for the oblate LoS cluster and therefore the Bayesian evidence does not prefer either the spherical or the triaxial model over the other.

In the case of the triaxial cluster simulations with odd axis in the plane of the sky, and hence elliptical iso-density contours, one would expect multiple spherical clusters to provide a better fit than just a single spherical cluster. This is confirmed by the evidence values as listed in Table 2. In fact, we fitted up to 4 spherical clusters for both prolate and oblate plane clusters and found the evidence value to be still increasing. We show the posterior distributions for the spatial coordinates at which the cluster is centred for the 1-spherical and 4-spherical model fits to the prolate and oblate plane clusters in Fig. 3. One can see multiple clusters aligned along the x -axis and y -axis, respectively, for the oblate and prolate plane clusters, which corresponds to the position angle of the projected iso-density contours in each case. It is clear from this figure that by fitting spherical NFW models to highly triaxial simulations, one would incorrectly infer the presence of multiple clusters. This is perhaps the biggest drawback of fitting spherical NFW models to intrinsically triaxial clusters and the most important result of this

| Cluster | Triaxial | 1-Spherical | 2-Spherical |
|---------------|-----------------|-----------------|-----------------|
| Prolate LoS | 636.1 ± 0.3 | 638.2 ± 0.3 | 632.6 ± 0.3 |
| Prolate Plane | 204.5 ± 0.3 | 163.4 ± 0.2 | 170.4 ± 0.3 |
| Oblate LoS | 111.8 ± 0.3 | 112.5 ± 0.3 | 107.6 ± 0.3 |
| Oblate Plane | 406.1 ± 0.3 | 346.7 ± 0.2 | 349.8 ± 0.3 |
| Spherical | 280.3 ± 0.2 | 280.6 ± 0.2 | 273.6 ± 0.3 |

Table 2. $\log Z$ values for fitting prolate LoS, prolate plane, oblate LoS, oblate plane and spherical clusters with triaxial (flat priors), one spherical cluster and two spherical cluster models.

study. It should also be noted that the single spherical cluster model is favoured in the analysis of the spherical NFW cluster simulation.

5 CONCLUSIONS

We have presented the weak lensing equations for the triaxial NFW profile. We also presented a method to estimate the cluster parameters assuming a triaxial NFW model. By considering four highly triaxial NFW galaxy clusters, we found that, spherical assumptions resulted in significant biases in parameter estimates for the cluster concentration C only for the prolate cluster in line-of-sight orientation. The cluster mass M_{200} was significantly biased, however, being overestimated for triaxial clusters oriented such that there is a lot of mass along the line-of-sight and underestimated for triaxial clusters with very little mass along the line-of-sight. The tension between the concentration $C \sim 4$ of clusters predicted in the Λ CDM model and the high values $C \sim 8$ estimated in some clusters when assuming a spherical model can therefore be explained if these clusters have very extreme axis ratios and oriented such that there is a lot of mass along the line-of-sight. Even more worryingly, the spherical model can lead to multiple cluster detections when applied to highly triaxial clusters with their odd axis in the plane of the sky. It is therefore important to be cautious in drawing conclusions about presence of substructure in weak gravitational lensing cluster studies in which a spherical cluster model has been used.

Even though our analysis algorithm is very efficient, fitting for triaxial cluster still takes a few days because, unlike the spherical case, the shear equations for triaxial NFW described in Sec. 3.2 do not have an analytical solution and need to be solved numerically. This makes the application of triaxial NFW model for searching large survey fields along the lines of the method presented in Feroz et al. (2008) unfeasible. In a future study, we plan to train an artificial neural network for solving these triaxial NFW equations and apply the resultant method on survey fields.

Another important area for studying cluster physics is through coherent analysis of weak/strong lensing, optical, X-ray and Sunyaev-Zel'dovich (SZ) observations. As we can see, analysis using weak lensing data only results in large uncertainties in cluster parameters due to inherent underconstrained nature of the problem. It is therefore important to perform a joint analysis using several different data-sets in order to obtain better constraints on cluster parameters. Marshall et al. (2003) presented a method for the joint analysis of lensing and SZ observations which was further extended in Feroz et al. (2009) and Hurley-Walker et al. (2011). These studies assumed a spherical NFW model. We plan to extend this to a triaxial NFW model and incorporate the X-ray observations as well in a future work.

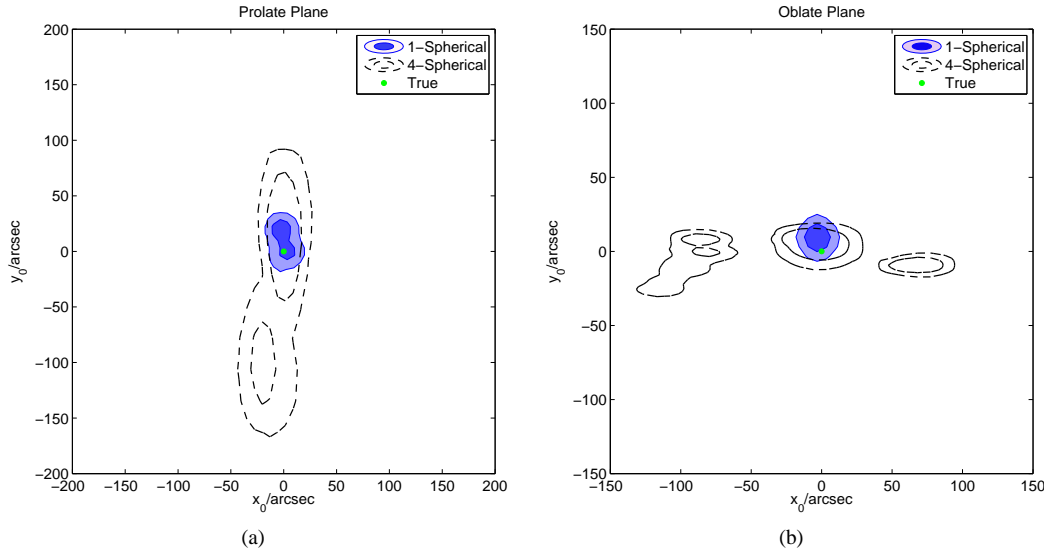


Figure 3. 2-D marginalized posterior probability distributions in the x_0 - y_0 plane for (a) prolate plane cluster, (b) oblate plane cluster, when analysed assuming 1 and 4 spherical cluster models.

ACKNOWLEDGEMENTS

We thank Lindsay King and James Mead for useful discussions regarding the triaxial NFW model lensing equations. This work was carried out largely on the COSMOS UK National Cosmology Supercomputer at DAMTP, Cambridge and the Darwin Supercomputer of the University of Cambridge High Performance Computing Service (<http://www.hpc.cam.ac.uk/>), provided by Dell Inc. using Strategic Research Infrastructure Funding from the Higher Education Funding Council for England. FF is supported by a Research Fellowship from Trinity Hall, Cambridge.

REFERENCES

- Bartelmann M., 1996, *A&A*, 313, 697
 Battye R. A., Weller J., 2003, *Phys.Rev.D*, 68, 083506
 Bett P., Eke V., Frenk C. S., Jenkins A., Helly J., Navarro J., 2007, *MNRAS*, 376, 215
 Bridle S. L., Hobson M. P., Lasenby A. N., Saunders R., 1998, *MNRAS*, 299, 895
 Corless V. L., 2008, PhD thesis, University of Cambridge
 Corless V. L., King L. J., 2007, *MNRAS*, 380, 149
 Corless V. L., King L. J., 2008, *MNRAS*, 390, 997
 Evrard A. E., MacFarland T. J., Couchman H. M. P., Colberg J. M., Yoshida N., White S. D. M., Jenkins A., Frenk C. S., Pearce F. R., Peacock J. A., Thomas P. A., 2002, *ApJ*, 573, 7
 Feroz F., Hobson M. P., 2008, *MNRAS*, 384, 449
 Feroz F., Hobson M. P., Bridges M., 2009, *MNRAS*, 398, 1601
 Feroz F., Hobson M. P., Zwart J. T. L., Saunders R. D. E., Grainge K. J. B., 2009, *MNRAS*, 398, 2049
 Feroz F., Marshall P. J., Hobson M. P., 2008, arXiv e-prints [arXiv:0810.0781]
 Fort B., Mellier Y., Dantel-Fort M., 1997, *A&A*, 321, 353
 Gavazzi R., 2005, *A&A*, 443, 793
 Gavazzi R., Fort B., Mellier Y., Pelló R., Dantel-Fort M., 2003, *A&A*, 403, 11
 Hobson M. P., McLachlan C., 2003, *MNRAS*, 338, 765
 Hoekstra H., Mellier Y., van Waerbeke L., Semboloni E., Fu L., Hudson M. J., Parker L. C., Tereno I., Benabed K., 2006, *ApJ*, 647, 116
 Hurley-Walker N., et al., 2011, arXiv e-prints [arXiv:1101.5912]
 Jenkins A., Frenk C. S., White S. D. M., Colberg J. M., Cole S., Evrard A. E., Couchman H. M. P., Yoshida N., 2001, *MNRAS*, 321, 372
 Jing Y. P., Suto Y., 2002, *ApJ*, 574, 538
 Keeton C. R., 2001, arXiv e-prints [arXiv:astro-ph/0102341]
 Kneib J., Hudelot P., Ellis R. S., Treu T., Smith G. P., Marshall P., Czoske O., Smail I., Natarajan P., 2003, *ApJ*, 598, 804
 Liddle A. R., 2007, *MNRAS*, 377, L74
 Limousin M., Richard J., Jullo E., Kneib J., Fort B., Soucail G., Elíasdóttir Á., Natarajan P., Ellis R. S., Smail I., Czoske O., Smith G. P., Hudelot P., Bardeau S., Ebeling H., Egami E., Knudsen K. K., 2007, *ApJ*, 668, 643
 Marshall P. J., Hobson M. P., Slosar A., 2003, *MNRAS*, 346, 489
 Massey R., Refregier A., Bacon D. J., Ellis R., Brown M. L., 2005, *MNRAS*, 359, 1277
 Massey R., Rhodes J., Ellis R., Scoville N., Leauthaud A., Finoguenov A., Capak P., Bacon D., Aussel H., Kneib J.-P., Koekemoer A., McCracken H., Mobasher B., 2007, *Nature*, 445, 286
 Navarro J. F., Frenk C. S., White S. D. M., 1997, *ApJ*, 490, 493
 Oguri M., Lee J., Suto Y., 2003, *ApJ*, 599, 7
 Oguri M., Takada M., Umetsu K., Broadhurst T., 2005, *ApJ*, 632, 841
 Press W. H., Schechter P., 1974, *ApJ*, 187, 425
 Schramm T., 1990, *A&A*, 231, 19
 Schramm T., Kayser R., 1995, *A&A*, 299, 1
 Seitz C., Schneider P., 1997, *A&A*, 318, 687
 Shaw L. D., Weller J., Ostriker J. P., Bode P., 2006, *ApJ*, 646, 815
 Sheth R. K., Mo H. J., Tormen G., 2001, *MNRAS*, 323, 1
 Skilling J., 2004, in Fischer R., Preuss R., Toussaint U. V., eds, American Institute of Physics Conference Series Nested Sampling, pp 395–405
 Trotta R., 2007, *MNRAS*, 378, 72
 White S. D. M., Navarro J. F., Evrard A. E., Frenk C. S., 1993,

Nature, 366, 429